Calibration of the Krishna District Surface Albedo with OLI-Landsat 8 Images

M Sudhakar[1], S Snigdha[2], S Naga Bhargavi[3]
[1,2,3]Assistant Professor
PSCMR College of engineering and Technology

Abstract - The surface albedo assumes an imperative part in the trades of vitality and mass in the planetary limit layer. Along these lines, changes in albedo influence the adjust of radiance and vitality at the surface, which can be recognized with its checking. Albedo resoluteness has been performed through sundry sensors, but there is not yet any publication dealing with albedo calculation procedures utilizing OLI (Operational Land Imager) - Landsat 8 images in the Krishna district region. The objective of the study is to present the procedures for computing the albedo with OLI images and map it in area of the Krishna District, Andhra Pradesh. Images of the year 2016-2017, path 142,143 and row 48,49 were culled. The data indispensable for calculating the albedo were extracted from each image metadata: additive and multiplicative terms of radiance, reflectance and sun elevation angle. There were immensely colossal distinctions between the albedo values of irrigated plots, waterbodies, and vegetation. The albedo obtained with OLI images provides more differentiation of the sundry types of land use, due to the substantial increase in the radiometric resolution of this incipient sensor

Keywords - Albedo, Landsat, Krishna District.

I. INTRODUCTION

Net radiation plays a rudimental role in biophysical processes involving exchanges of energy and mass in the planetary edge-(from the same origin or family) layer, since it makes up the main energy source used in the heating of soil and air, and in plant evapotranspiration (Silva et al., 2005a; Wang & Davison, 2007; Giongo et al., 2010; Runs et al., 2013; Souza et al., 2014).Surface albedo (in a very huge) affects net radiation; this way, many satellites carry sensors that decide and monitor the Earth's surface albedo. Ergo, it's optically supervising has more and more gained most importantly, since the changes in fortune caused by natural andr anthropic (most important events or patterns of things) on the surface of the planet can be detected by orbital sensors, besides the role played by the albedo in ((from the same origin or family) to the Earth's weather) modelling.

There are different sets of computer instructions for the calculation of surface albedo that use radiometric (measuring things exactly) of AVHRR bands 1 and 2, some of which relate the (related to ghosts or the colors of the rainbow) planetary reflectance of these bands to the surface albedo (Wydick et al., 1987; Hucek & Jacobowitz, 1995). More (not very long ago), Liang (2000) received, for assorted different orbital sensors, equations that sanction calculating the albedo through the linear accumulation of the (based on only one color) reflectivity of each one of these bands in the solar radiation domain. Souza et al. (2014) applied the parameterization proposed by Tasumi et al. (2008) with high and low loadings of tiny solids mixed in with a gas in different areas of Brazil and data of the MODIS sensor. However, the model proposed by Zhong & Li (1988) employed by Bastiaanssen et al. (1998) in the SEBAL (Surface Energy Balance Set of computer instructions for Land) and at first applied to TM - Landsat 5 images, combines simpleness and (high) quality This model has been widely used in many studies on the balance of radiation, energy and in researches carefully studying changes in land use. The albedo has with also been used in (related to the Earth's weather) modeling and Krayenhoff & Voogt (2010) studied its influence on air temperature, while Wang & Davison (2007) (figured out the worth, amount, or quality of) the effect of (related to the Earth's weather) different things than different versions of the albedo of mild. Loew & Govaerts (2010), (figured out the worth, amount, or quality of) the consistency of long-term albedo data received with the Meteosat First Generation, used in (related to the Earth's weather) modeling. In (combination of different things together that work as one unit), it should be pointed out the role of cloud albedo in (related to the Earth's weather) supervising and analysis studied by Mueller et al. (2011).

In most studies using TM and ETM+, absolutely in applications of radiation and energy balance, the albedo is, at first, received through accumulations of (related to carefully think about past events) bands without (related to the air outside) rectification and then the (related to the air outside) effects are (corrected or made up for past events that were mean or unfair) based on the creation proposed by Zhong & Li (1988), intensively used by Bastiaanssen et al. (1998). More (not very long ago), Tasumi et al. (2008) developed a set of computer instructions for the (related to the air outside) rectification of each one of the TM and MODIS (mirror- related to carefully think about past events) bands, but based on the same rectification model proposed by Zhong & Li (1988). The main difference is that in, the last thing just mentioned the rectification is performed in the planetary albedo, while in the former the (related to the air outside) rectification is performed band to band, received through a radioactive move (from one place to another) model. This is the method adopted by the METRIC (Mapping Evapotranspiration with (made a part of you) (an adjustment for accuracy)), a different version of the SEBAL

and used in areas of mountains (Allen et al., 2007; Tasumi et al., 2008).

II. MATERIALS AND METHODOLOGY

Eight OLI-Landsat 8 images, path 143 and row 47,48, generated between 22-11-2015 to 06-01-2016, having an interval of 16days temporal resolution are obtained from the United States Geological Survey – USGS (http://earthexplorer.usgs.gov/) were used in the study. These images correspond to the Landsat 8 overpass approximately at 05 h 03 min (local time), and have spatial resolution of 30 m and spectral resolution of 12 bits, but are available in 16 bits, which means an intensity in each pixel between 0 and 65,535 grey levels, ensuring a higher detailing degree of the generated information. In addition, meteorological data recorded close to the Landsat 8 pass over the studied area were used, to determine the atmospheric transmittance used in the atmospheric correction. The selected days and the data used in the image processing are shown in Table 2.

The albedo was calculated using the following equation (Bastiaanssen et al., 2002):

$$\propto = \frac{\propto_{toa} - \propto_{atm}}{\tau_{sw}} \qquad (1)$$

Where:

αtoa - Planet albedo of each pixel or albedo without atmospheric correction;

αatm - atmospheric albedo, 0.03 based on Bastiaanseen (2000); and

τsw - atmospheric transmittance in the solar radiationdomain, which can be obtained by the equation (Allen et al.,2002, 2007)

$$\tau_{sw} = 0.75 + 2 * 10^{-5} Z \qquad (2)$$

where

Z = elevation of the weather station from mean sea level

The value of atmospheric albedo can be obtained through a radiative transfer model and, in general, is situated between 0.025 and 0.040 (Allen et al., 2002). The value of 0.03 was adopted in the present study. The determination of albedo without atmospheric correction (αtoa) was performed through linear combination of the monochromatic reflectance (rb) of the reflective bands (from 2 to 7) of the OLI - Landsat 8 (Eq. 4), according to the following equation:

αtoa = p2 x r2 + p3 x r3 + p4 x r4 + p5 x r5 + p6 x r6 + p7 x r7 (3)

where the reflectance of each one of the bands (from 2 to 7) was obtained by Chander & Markham (2003):

$$r_b = \frac{\mathrm{Add_{ref,b}} + \mathrm{Mult_{ref,b}} \mathrm{ND}}{\mathrm{CosZd_r}} \qquad (4)$$

where:

Addref,b and Multref,b - represent additive and multiplicative terms of the reflectance of each band, extracted from the metadata of each image (group = radiometric_rescaling), as well as the Sun zenith angle - Z;

NDb - intensity of each pixel and band (value between 0 and 65365);

b - subscript representing each one of the Eight OLI bands; and

dr - corresponds to the correction of the eccentricity ofthe terrestrial orbit, given by:

$$d_r = \left(\frac{1}{d_{ES}}\right) \qquad (5)$$

dES - Earth-to-Sun distance (astronomic unit) on the dayof each image, also extracted from the metadata

For the determination of each weight (pb), it is necessaryto estimate the solar constant (Kb, W m-2 μm-1) associated with each one of the OLI reflective bands and, for this, the Eq. 6 was used according to Chander & Markham (2003).

$$k_b = \frac{\pi L_b}{r_b cos Z d_r} \qquad (6)$$

where:

Lb (W m-2 sr-1 μm-1) - radiance of each pixel of the b-bandand the other terms have already been described.

For the determination of the Lb of each pixel and band, theadditive (Addrad,b) and multiplicative (Multrad,b) terms relative to the radiance were used, also extracted from the metadata of each image, calculated according to the equation:

$$Lb = Addrad,b + Multrad,b NDb \qquad (7)$$

The value of each weight (Pb) of each spectral band was obtained by the ratio between the kb of that band and the sum of all the kb values used in the calculation of the albedo, like what has been done in the SEBAL and METRIC (Bastiaanssen et al., 1998; Allen et al., 2007; Tasumi et al., 2008).

Table 2. Variables used in albedo calculation for the studied area: Sun elevation angle - E (degree), cosine of the Sun zenith angle - cos Z, and atmospheric transmittance - τoc, referring to the moment of the satellite overpass on the days selected for the study, and Earth-to-Sun distance - dES (astronomic unit) in each selected day(DOY)For determining αtoa we need to calculate each band of image (according to equation 3) it's become a complex process to calculate so developed a model as shown in the fig 2 in Arcmap 10.3. Model by four part, initial Calculation of Reflectance and radiance of image from band 2 to band 7 with help of Meta data. The output of both image of radiance and reflectance given to computing input of solar constant. Finally Planet albedo generated by radiance and weight coefficient, with help of raster calculator surface albedo thematic map generated

There are different techniques for the determination of surface albedo through orbital images. However, the most used one with Landsat images in researches involving radiation and energy balances. This method requires the identification of the weights or relative contribution of each spectral band in the composition of the albedo in the entire solar radiation spectrum, which is widely known

(Bastiaanssen el al., 1998; Allen et al., 2002; 2007; Silva et al., 2005a,b). For Landsat 8, these weights have not yet been published and one of the objectives of this study is their determination, specifically for OLI. For this, the specific solar constant (Kb) of each one of the OLI bands from 2 to 7 was obtained based on Eq. 6. The values of Kb (W m-2 μm-1 sr-1) for the four selected days of five images are shown in Figure 10 to 15

The Computed each pixel Radiation was show in Figure 1 to 4. The observed change is Depending by the DOI. The computed each pixel Reflectance value was show in figure 5 to 9 and calibrated solar constant was show in figure 10 to 14 and determined Weights for Band 2 to Band 7 value of each pixel was show 15 to 20. The TOA and Albedo of various DOI was show in Figure 21 and 22. For observing albedo variation of different location observed by to selection of 124 point for Roads, which is show in figure 25, 200 point for vegetation which is show in figure 23, 71 point for Waterbodies, which is show in figure 24 and observed 6 industrials variation of albedo show in figure 31. The linear variation of Albedo observed by each pixel which is constructed the graph was show in Figure 26,27, 27 and 28

III. CONCLUSION

The Albedo of irrigated areas was more clearly different from native vegetation areas in months that are further away from the rainy season. Albedo images show great degree of detail for the different types of land use and occupation, due to their high radiometric resolution.

We observed the various change in albedo value with respect to three months, which are November, December and February. The Landsat8 30m resolution helps to identify the different feature in ground. We also observed in month Maximum February due to obstruction water bodies, Vegetation and Road are subject high albedo value.

We selected 200 Vegetation points in Krishna district. These results are various spastically and temporally due to water availability of land typical crop system Vegetation in the month of December have low albedo value which means that high vegetation in the region of Krishna district.

We selected 71 Water bodies in Krishna district. These results are various spastically and temporally due to moment of cloud and temperature. We selected 6 Industries in Krishna district. These results are various spastically but not temporally which means albedo value is likely constant due to emission of heat from industries, show in Figure 29

We selected 124 Roads in Krishna district. This result is various spastically and temporally which means albedo increase due to urban area. the metal road of urban area emits more radiation

Finally, this will help to understand radiation changes in environment

IV. REFERENCES

[1]. Allen, R. G.; Tasumi, M.; Trezza, R. Satellite-based energy balance for mapping evapotranspiration with internalized calibration (METRIC) - Model. Journal of Irrigation and Drainage Engineering, v.133, p.380-394, 2007. http://dx.doi.org/10.1061/ (ASCE)0733-9437(2007)133:4(380

[2]. Allen, R. G.; Trezza, R.; Tasumi, M. Surface energy balance algorithms for land. Advance training and user's manual, version 1.0. Kimberly: The Idaho Department of Water Resources, 2002. 98p

[3]. Bastiaanssen, W. G. M.; Menenti, M.; Feddes, R. A.; Holslag, A. A. M. A. Remote sensing surface energy balance algorithm for land (SEBAL) - Formulation. Journal of Hydrology, v.212-213, p.198212, 1998. http://dx.doi.org/10.1016/S0022-1694(98)00253-4

[4]. Bezerra, J. M.; Moura, G. B. de A.; Silva, B. B. da; Lopes, P. M. O.; Silva, E. F. de F. e. Parâmetros biofísicos obtidos por sensoriamento remoto em região semiárida do estado do Rio Grande do Norte, Brasil. Revista Brasileira de Engenharia Agrícola e Ambiental, v.18,p.123-130,2014. http://dx.doi.org/10.1590/S14154366201400010010

[5]. Chander, G.; Markhan, B. Revised Landsat 5 - TM radiometric calibration procedures and post calibration dynamic ranges. IEEE Transactions on Geosciences and Remote Sensing, v.41, p.2674-2677, 2003. http://dx.doi.org/10.1109/TGRS.2003.818464

[6]. Chander, G.; Markham, B. L.; Helder, D. L. Summary of current radiometric calibration coefficients for Landsat MSS, TM, ETM+, and EO-1 ALI sensors. Remote Sensing of Environment, v.113, p.893-903, 2009. http://dx.doi.org/10.1016/j.rse.2009.01.007

[7]. Giongo, P. R.; Moura, G. B. A.; Silva, B. B. da; Rocha, H. R. da; Medeiros, S. R. R. de; Nazareno, A. C. Albedo à superfície a partir de imagens Landsat 5 em áreas de cana-de-açúcar e cerrado. Revista Brasileira de Engenharia Agrícola e Ambiental, v.14, p.279-287, 2010. http:// dx.doi.org/10.1590/S1415-43662010000300007

[8]. Hucek, R.; Jacobowitz, H. Impact of scene dependency on AVHRR albedo models. Journal of Atmospheric and Oceanic Technology, v.12, p.697-711, 1995. http://dx.doi.org/10.1175/15200426(1995)012%3C0697:IOSDOA%3E2.0.CO

[9]. Liang, S. Narrowband to broadband conversions of land surface albedo I Algorithms. Remote Sensing of Environment, v.76, p.213238, 2000. http://dx.doi.org/10.1016/S0034-4257(00)00205-4

[10]. Lopes, P. M. O.; Valeriano, D. de M.; Silva, B. B. da; Moura, G. B. A.; Silva, A. O. Simulação do saldo de radiação na Serra da Mantiqueira. Revista Brasileira de Engenharia Agrícola e Ambiental, v.17, p.780-789, 2013. http://dx.doi.org/10.1590/S1415-43662013000700013

[11]. Machado, C. C. C.; Silva, B. B. da; Albuquerque, M. B.; Galvíncio, J. D. Estimativa do Balanço de energia utilizando imagens TM - Landsat 5 e o algoritmo SEBAL no litoral sul de Pernambuco. Revista Brasileira de Meteorologia, v.29,p.55,2014.

[12]. Oliveira, L. M. M.; Montenegro, S. M. G. L.; Antonino, A. C. D.; Silva, B. B. da; Machado, C. C. C.; Galvíncio, J. D. Análise quantitativa de parâmetros biofísicos de bacia hidrográfica, obtidos por sensoriamento remoto. Pesquisa Agropecuária Brasileira, v.47, p.1209-1217, 2012.

[13]. Silva, B. B. da; Bezerra, M. V. C. Determinação dos fluxos de calor sensível e latente na superfície utilizando imagens TM - Landsat 5. Revista Brasileira de Agrometeorologia, v.14, p.174-186, 2006.

[14]. Wydick, J.; Davies, P.; Gruber, A. Estimation of broadband planetary albedo from operational narrowband satellite measurements. Washington: National Oceanic and Atmospheric

Administration, 1987. 32p, NOAA Technical Report, NESDIS 27

[15]. Zhong, Q.; Li, Y. H. Satellite observation of surface albedo over the Qinghai-Xizang plateau region. Advances in Atmospheric Science, v.5, p.57-65, 198

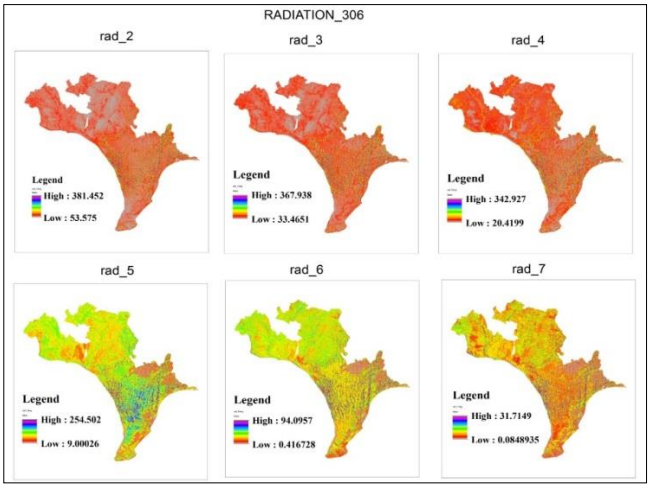

Figure 1 Radiation DOI 306

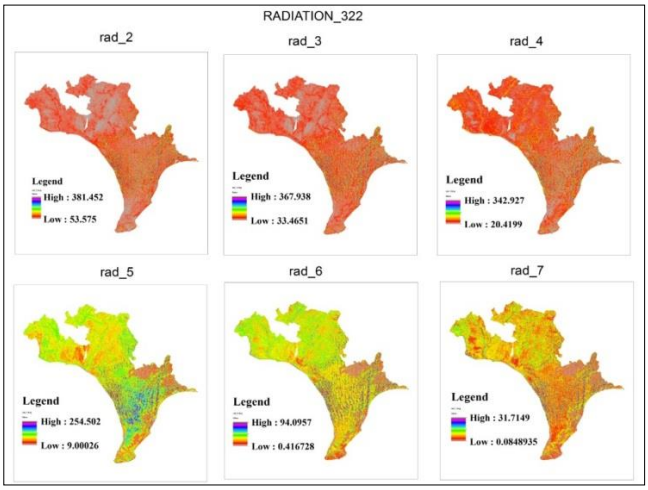

Figure 2 Radiation DOI 322

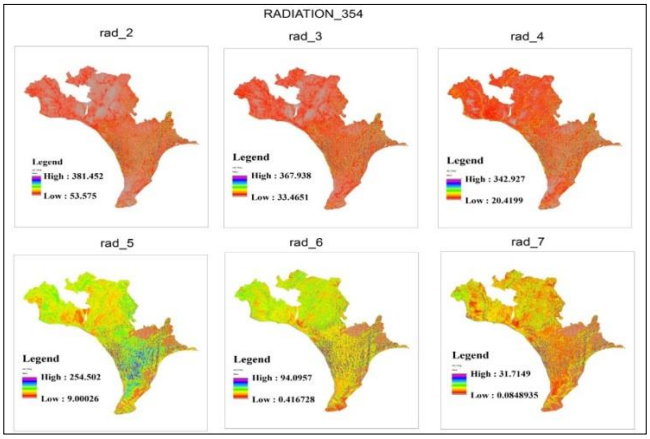

Figure 3 Radiation DOI 354

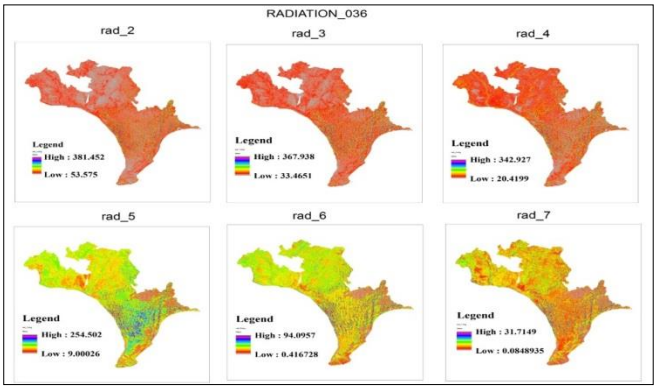

Figure 4 Radiation DOI 36

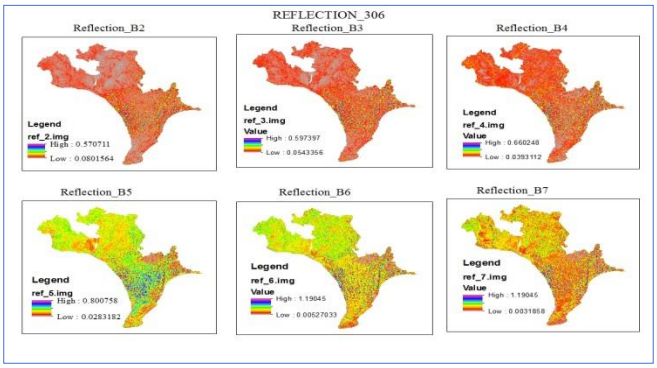

Figure 5 Reflection DOI 306

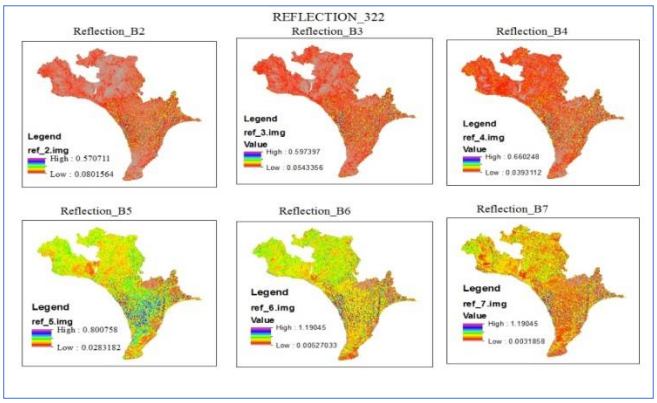

Figure 6 Reflection DOI 322

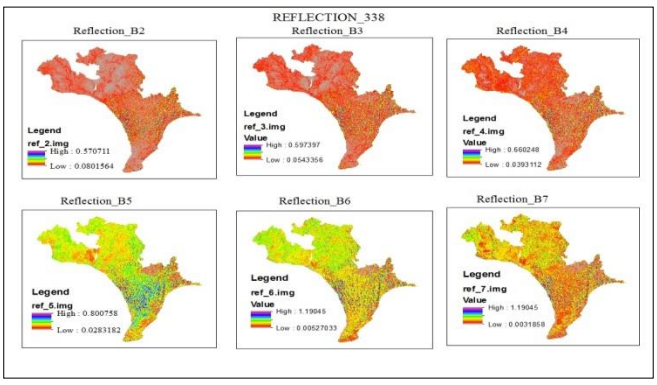

Figure 7 Reflection DOI 338

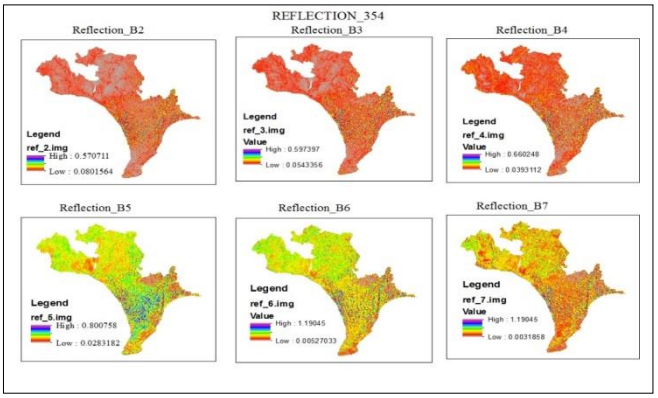

Figure 8 Reflection DOI 354

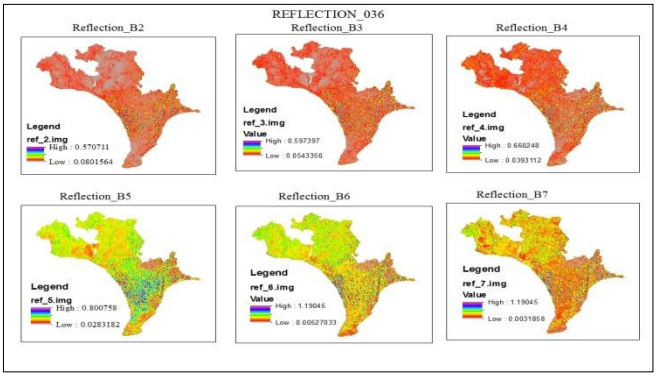

Figure 9 Reflection DOI 36

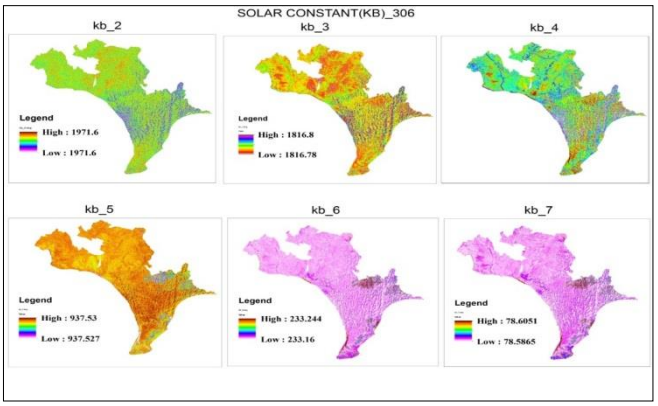

Figure 10 solar oonstant DOI 306

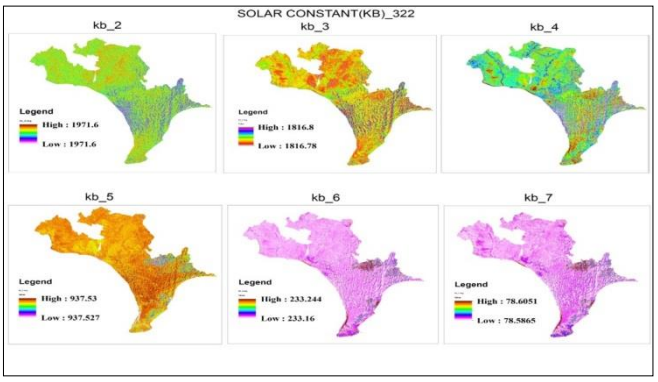

Figure 11 solar oonstant DOI 322

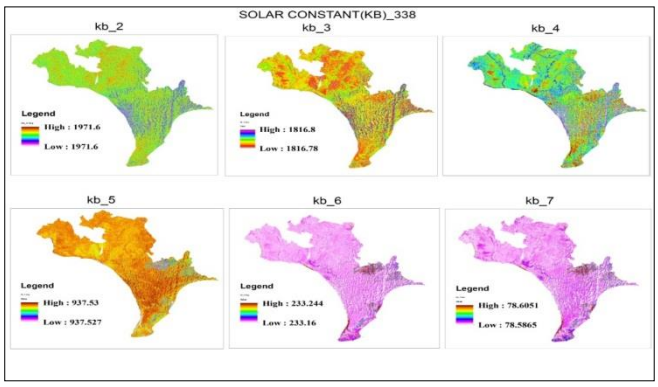

Figure 12 solar constant DOI 338

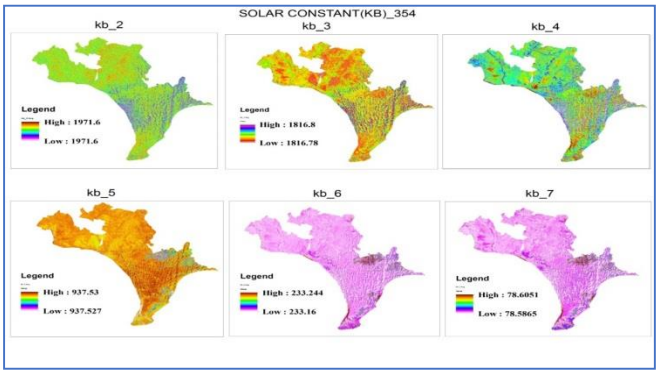

Figure 13 solar constant DOI 354

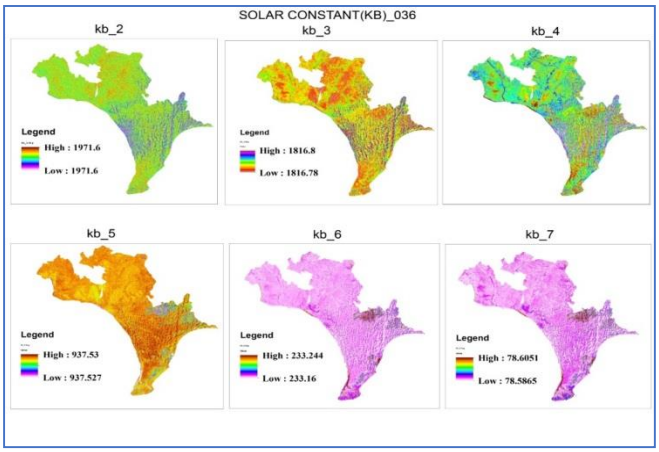

Figure 14 solar oonstant DOI36

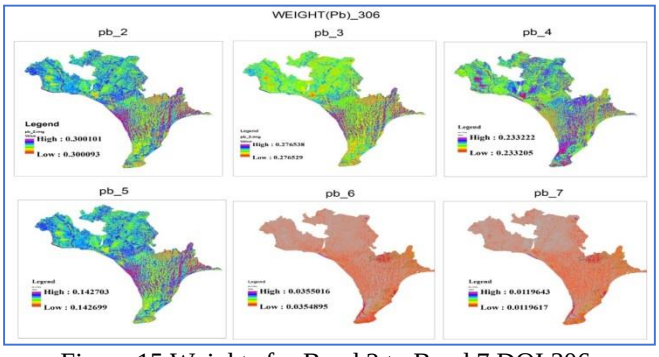

Figure 15 Weights for Band 2 to Band 7 DOI 306

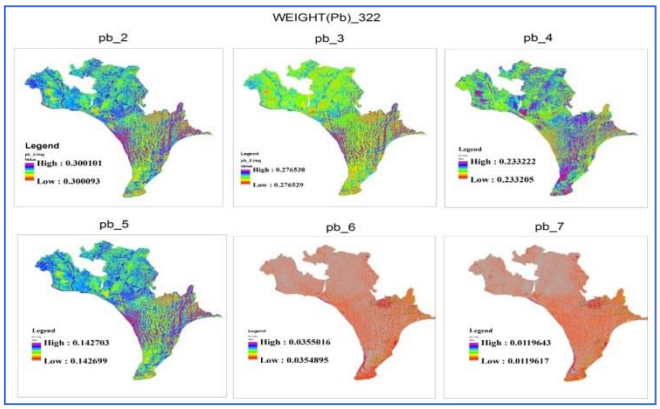

Figure 16 Weight for Band 2 to Band 7 DOI 322

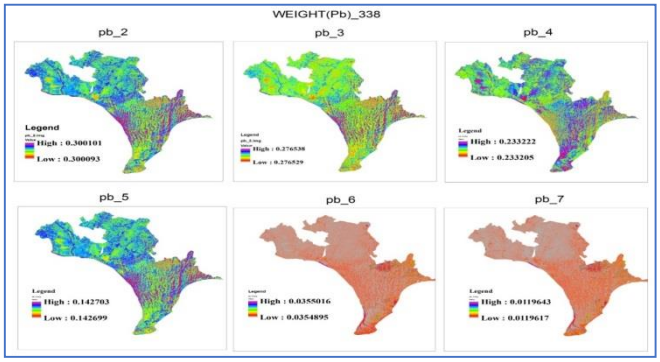

Figure 17 Weight for Band 2 to Band 7DOI 338

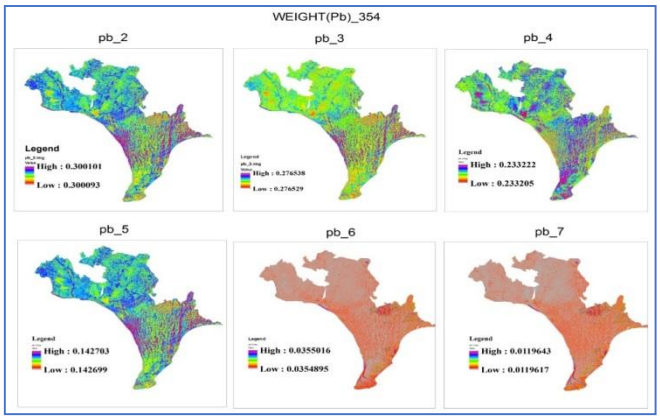

Figure 18 Weight for Band 2 to Band 7 DOI 354

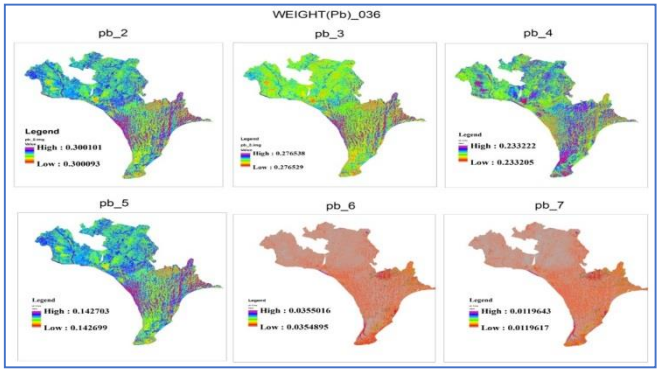

Figure 19 Weight for Band 2 to Band 7DOI 36

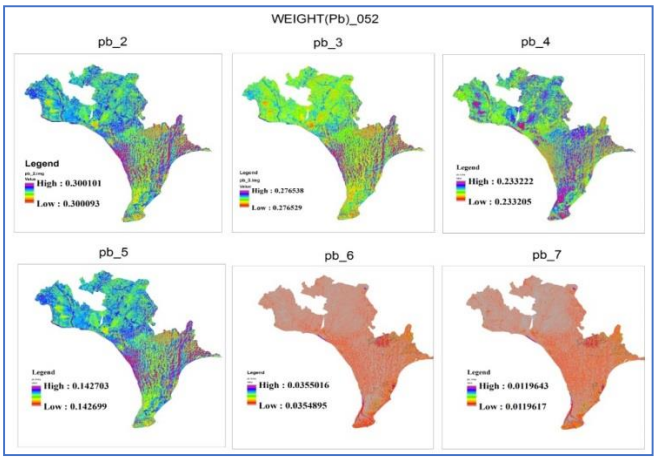

Figure 20 Weight for Band 2 to Band 7DOI 52

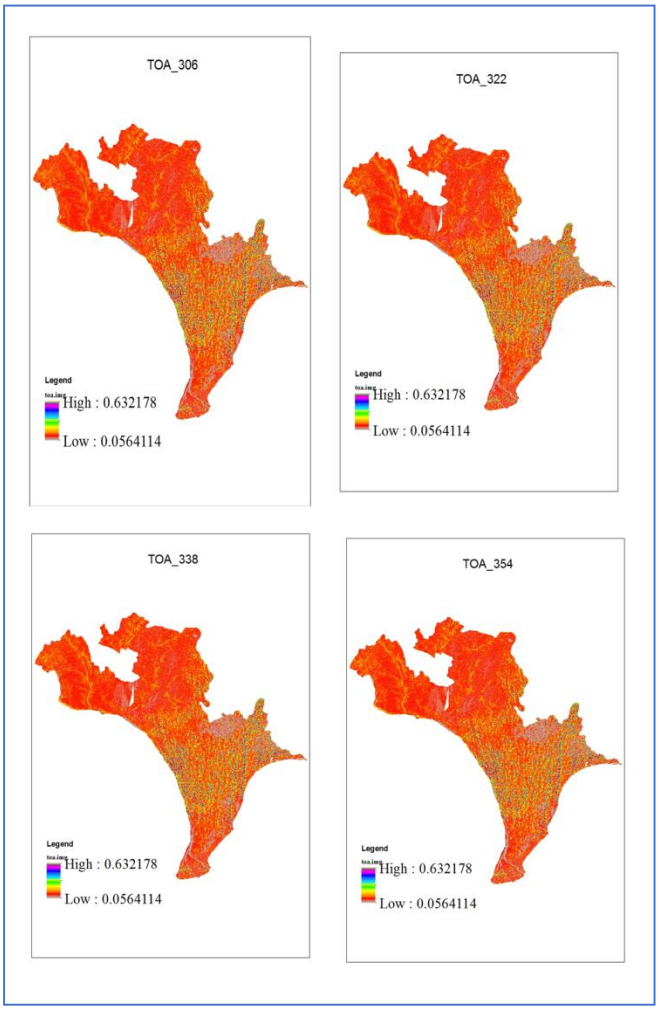

Figure 21 TOA DOI of 306, 322, 338, 354

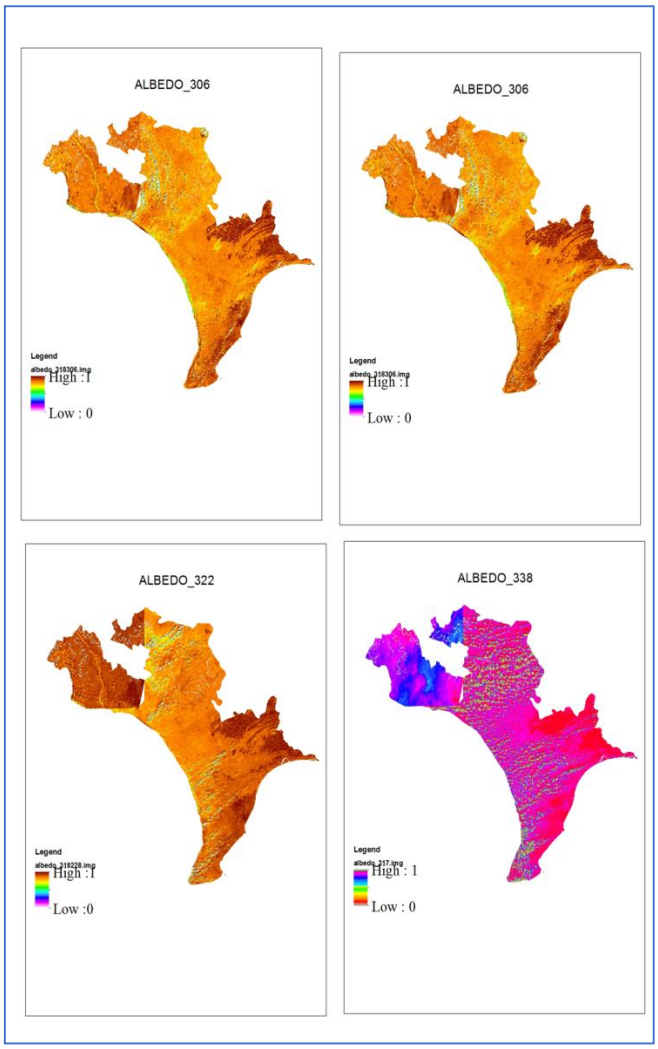

Figure 22Albedo DOI of 306, 322, 338, 354

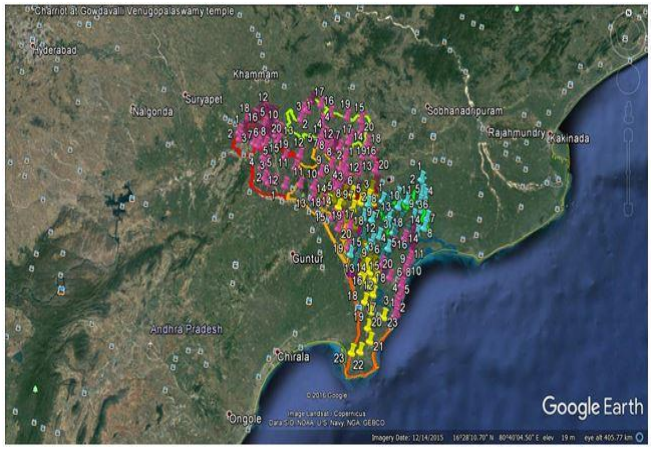

Figure 23 Selected Vegetation Point in Krishna district

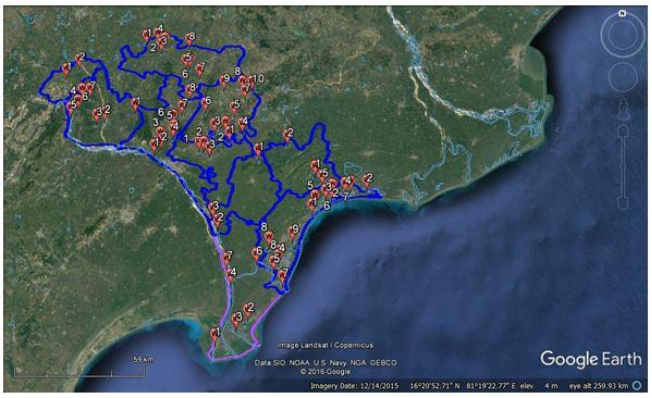

Figure 1 Selected Waterbodies Point in Krishna River

Figure 25 Selected Road Point in Krishna district

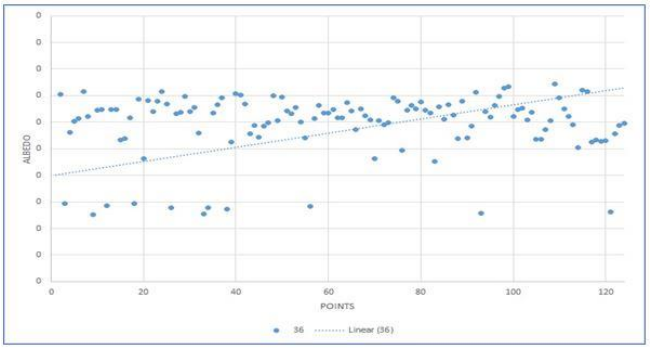

Figure 2 Albedo of River vs Seleceted Point for DOI 36

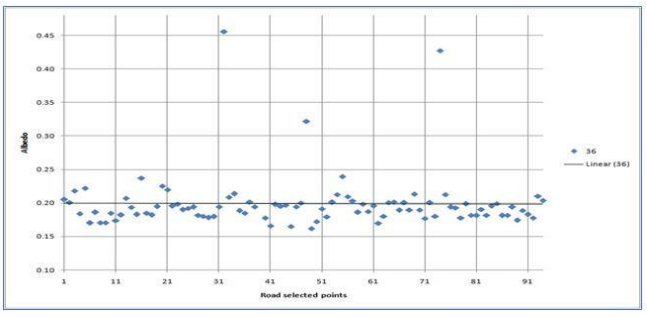

Figure 27 Alebdo of Road vs Selected point for DOI 36

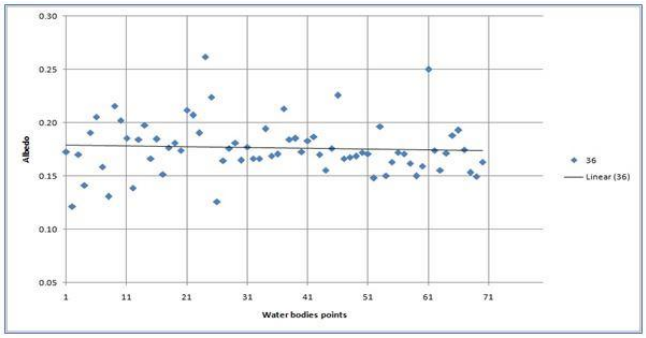

Figure 3 Albedo of Waterbodies vs Selected points for DOI 36

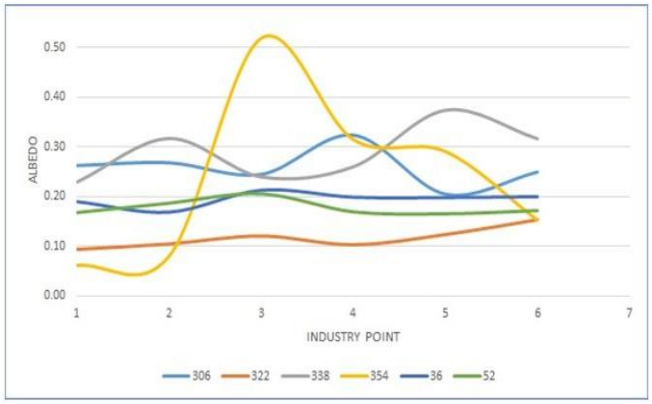

Figure 4 Albedo industrie for diffent DOI vs seleced industries